Journal of Biomedical Optics

BiomedicalOptics.SPIEDigitalLibrary.org

Investigation of optical properties of dissected and homogenized biological tissue

Maximilian Eisel
Stephan Ströbl
Thomas Pongratz
Herbert Stepp
Adrian Rühm
Ronald Sroka

SPIE.

Maximilian Eisel, Stephan Ströbl, Thomas Pongratz, Herbert Stepp, Adrian Rühm, Ronald Sroka, "Investigation of optical properties of dissected and homogenized biological tissue," *J. Biomed. Opt.* **23**(9), 091418 (2018), doi: 10.1117/1.JBO.23.9.091418.

Investigation of optical properties of dissected and homogenized biological tissue

Maximilian Eisel,[a,b,*] Stephan Ströbl,[a,b] Thomas Pongratz,[a,b] Herbert Stepp,[a,b] Adrian Rühm,[a,b] and Ronald Sroka[a,b]
[a]Klinikum der Universität München, Laser-Forschungslabor, LIFE-Zentrum, Munich, Germany
[b]University Hospital of Munich, Department of Urology, Munich, Germany

Abstract. Knowledge of tissue optical properties, in particular the absorption μ_a and the reduced scattering coefficient μ_s', is required for diagnostic and therapeutic applications in which the light distribution during treatment has to be known. As it is generally very difficult to obtain this information with sufficient accuracy *in vivo*, optical properties are often approximately determined on *ex vivo* tissue samples. In this case, the obtained optical properties may strongly depend on the sample preparation. The extent of the expectable preparation-dependent differences was systematically investigated in comparative measurements on dissected and homogenized porcine tissue samples (liver, lung, brain, and muscle). These measurements were performed at wavelengths 520, 635, 660, and 785 nm, using a dual-step reflectance device and at a spectral range of 515 to 800 nm with an integrating sphere setup. In a third experiment, the density of tissue samples (dissected and homogenized) was investigated, as the characteristic of the packaging of internal tissue structures strongly influences the absorption and scattering. The standard errors of the obtained absorption and reduced scattering coefficients were found to be reduced in case of homogenized tissue. Homogenizing the tissues also allows a much easier and faster sample preparation, as macroscopic internal tissue structures are destroyed in the homogenized tissue so that a planar tissue sample with well-defined thickness can easily and accurately be prepared by filling the tissue paste into a cuvette. Consequently, a better reproducibility result was obtained when using homogenized samples. According to the density measurements accomplished for dissected and homogenized tissue samples, all types of tissues, except lung, showed a decrease in the density due to the homogenization process. The presented results are in good agreement for μ_s' regardless of the preparation procedure, whereas μ_a differs, probably influenced by blood content and dehydration. Because of faster and easier preparation and easier sample positioning, homogenization prior to measurement seems to be suitable for investigating the optical properties *ex vivo*. Additionally, by means of using the homogenization process, the sample size and thickness do not need to be particularly large, as is the case for most biopsies from the OR. [DOI: 10.1117/1.JBO.23.9.091418]

Keywords: optical properties; biological tissue; spatially resolved reflectance; total diffuse reflectance; integrating sphere; density measurements.

Paper 170778SSPRRR received Dec. 1, 2017; accepted for publication Aug. 30, 2018; published online Sep. 24, 2018.

1 Introduction

Optical diagnostic and therapeutic applications usually depend on knowledge of the light distribution in the treated area, for instance in photodynamic therapy (PDT)[1–3] and diagnosis (PDD),[4,5] photocoagulation,[6,7] and fluorescence diagnosis in general.[8,9] The light distribution in turn depends on the optical tissue properties (μ_a, μ_s) and their distribution in space.[10–12] There are several photometric techniques (direct and indirect) available for measurement of optical properties. Direct measurements (thin sample, single scattering events) focus on one particular microscopic coefficient and normally do not use a model for light propagation. Indirect methods (thick sample and multiple scattering) calculate the macroscopic optical parameters via an inverse model [inverse adding doubling (IAD), diffusion approximation] from measured quantities (e.g., diffuse/collimated reflection or transmission).[13] The estimation of optical properties of extracted biological tissues is often performed by single- or double-integrating sphere (IS) technique.[14–20] Another approach is to exploit the backscattered light from a thick sample surface either for absolute measurement or spatially resolved evaluation.[21–27] In a modified form, backscattered light can be also used for time resolved,[28] frequency domain,[29] and spatial-frequency domain[30] measurements, and finally also using OCT-technology.[31] Furthermore, such techniques have the potential to be adjusted to clinical applications.

Biological tissue, however, does usually not show uniform optical properties within a macroscopic volume as it contains regions made up of different types of cells, connective tissue, vessels, and boundary layers, such as an organ capsule (serous membrane) or membranes.[32–35] As well, natural degradation of the tissue samples and the related changes in pH, moisture, and oxygenation have to be taken into account.[12] Precise and reproducible slicing of the tissue to investigate the optical properties by IS techniques is challenging, and often the fixing compounds used in preparation must be taken into account.[36] Shredding the tissue causes most of its internal structures to be destroyed or more evenly distributed,[10] thus creating a macroscopic volume with rather uniform optical properties. Although studies concerning the comparison of different measurement techniques

*Address all correspondence to: Maximilian Eisel, E-mail: Max. Eisel@med.uni-muenchen.de

1083-3668/2018/$25.00 © 2018 SPIE

are available and a lot of investigations into tissue mimicking phantoms (layered and homogenous) are performed,[37–40] the influence of the structure of tissue sample on the optical properties has not been investigated systematically on biological samples so far. Thus, the objective of this investigation is the comparison of the optical properties measured on dissected, sliced tissue samples and their corresponding homogenized versions using the IS technique and a dual-step reflectance method (DSR). Both employed methods use mathematical approximations, like the radiative transfer equation, in combination with homogeneous optical tissue properties to calculate the optical properties from reflection or transmission measurements on the illuminated sample. These approximations often rely on simplifying assumptions about the investigated tissue volume, such as homogeneity of the optical tissue properties.[6]

In addition to evaluating whether the homogenizing process is suitable to obtain at least similar optical properties values by using dissected tissue samples, or whether the interference is too harsh to the tissue's structure, a simplification and thus time-saving aspect of the tissue preparation process accompanied by an increase of reproducibility should be tested. In particular the method of homogenizing is very interesting for small, heterogeneous, or traumatized samples from biopsies or resections (e.g., cholesteatoma[41] and glioblastoma[42]). As the optical properties of *ex vivo* samples highly depend on the storage conditions and further processing[7,11,32,43] and may thus decidedly differ from those of *in vivo* tissue, future work should be focused on the relation between these two kinds of state of tissue conditions.

2 Materials and Methods

2.1 *Samples and Sample Preparation*

Measurements, performed on porcine brain, liver, lung, and muscle from the abattoir, were used within 48 h after sacrifice, representing heterogenic pasty, bloody, uncongested, and structured conditions, respectively. The samples were stored in a refrigerator in separated plastic containers at a temperature of 4°C until experiments. For DSR measurements, the tissue samples (dissected: Ø: ~40 mm; homogenized Ø: ~80 mm) were placed into plastic Petri dishes (Ø: 80 mm; height: 25 mm). A sample thickness of ~10 mm was chosen to prevent light interaction with the bottom of the Petri dish. An even sample surface was imperative for reproducible measurement results. Tissue homogenization[10] was accomplished using a commercial hand blender (STUDIO St10, Sertronics GmbH, Saarlouis, Germany) for 2 min at ~12,000 rpm (power mode II). IS measurements were performed on samples dissected into rectangular slices with at least 30-mm edge length and a thickness of 1 mm. The tissue slices were positioned between two microscope slides (50 mm × 50 mm × 1 mm) separated by 1-mm-thick spacers. In this way, a squeezing of the sample between the glass slides was avoided and a defined thickness could be obtained to prevent an unwanted alteration of the scattering and absorption coefficients.[6,32] The homogenized tissue paste was equally distributed on a glass slide and covered by a second glass slide with the 1-mm spacer in between. Careful positioning guaranteed minimal squeezing of the tissue paste.

The sample preparation (dissection/homogenizing) took place immediately before measurement, hence guaranteeing reproducible tissue conditions.

2.2 *Experimental Setups*

2.2.1 *Dual-step reflectance measurement*

The determination of optical properties was accomplished by (a) spectral measurement of the total diffuse reflectance of the tissue surface using a broadband white-light source and (b) detecting the spatially resolved diffuse reflectance from the tissue surface illuminated with a monochromatic laser beam in a sharply defined spot via a CCD camera. These two procedures were condensed to one setup, termed DSR setup. This setup is described in the following.

The spectral measurement of the total diffuse reflectance of the tissue surface was performed by perpendicular illumination of the sample surface by a halogen white-light source (Xenophot, Osram, Germany) coupled into an optical fiber ($Ø_{core}$: 1000 μm, NA: 0.37), as shown in Fig. 1. The achromatic lens ($f = 5$ mm) at the distal end of the optical fiber ensures a uniform light distribution within a circular spot on the tissue surface ($Ø_{spot}$: 20 mm). The remitted light is collected by means of a second optical fiber ($Ø_{core}$: 600 μm, NA: 0.37), which is aligned under 45 deg with respect to the tissue surface. The polished flat end of this detection fiber is positioned at a distance of 50 mm to the intersection point of the fiber axis and the sample surface. To obtain correct results, it has to be ensured that the surface area from which remitted light is collected into the detection fiber is fully contained within the homogeneously illuminated spot on the tissue surface. The detection fiber guides the collected light to a spectrometer (S2000, Ocean Optics, Ostfildern, Germany). The spectrometer is sensitive in the spectral range from 200 to 850 nm. For each measurement a reference spectrum was taken, using a Lambertian reflectance standard (SG3060/7, Ø: 30 mm, reflectance: 30%, L.O.T. – Oriel GmbH & Co. KG, Darmstadt, Germany) using the same geometrical setup. The software OOIBASE (Ocean Optics, Dunedin, Florida) was used to visualize and save the respective spectra of sample and standard.

By measuring the remitted light intensities of the tissue sample ($I_{sample}, I_{standard}$) in comparison with the Lambertian remission standard R_s, the total diffuse reflectance R of the sample surface can be evaluated according to Eq. (1):

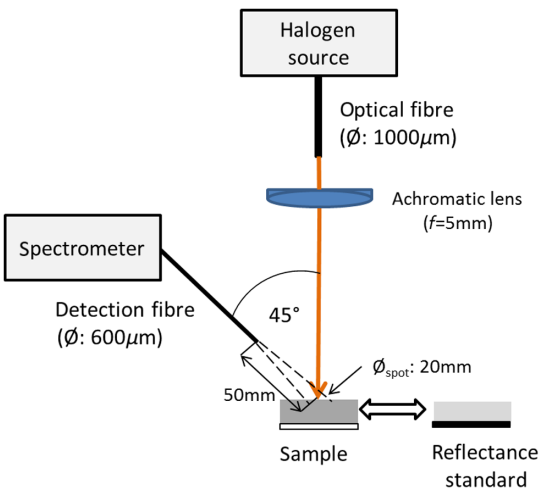

Fig. 1 Spectral total diffuse reflectance measurement setup comprising a fiber-coupled halogen lamp and a 45-deg inclined detection fiber attached to a spectrometer.

$$R = \frac{I_{\text{sample}}}{I_{\text{standard}}} \cdot R_{\text{standard}}. \tag{1}$$

In approximation the following equation can be used:[44]

$$R \approx \exp\left[-\frac{A(q)}{\sqrt{3\left(1+\frac{1}{q}\right)}}\right], \tag{2}$$

where

$$q = \frac{\mu_a}{\mu_s'}, \tag{3}$$

denotes the quotient of the sample's absorption and reduced scattering coefficient. The function $A(q)$ additionally depends on the relative refractive index $n_{\text{rel}} = \frac{n_{\text{surrounding}}}{n_{\text{sample}}}$, and can be determined by Monte Carlo simulations. By inverting Eq. (2) via lookup tables and interpolation, the quotient q can be calculated for any experimentally obtained values of R_d.

For the spatially resolved reflectance measurement, a monochrome CCD camera (SensiCam Long Exposure, PCO Computer Optics GmbH, Kelheim, Germany) was used to record the spatial intensity distribution on the sample surface while irradiated with a narrow laser beam. The employed setup allowed the determination of optical properties at four specific fixed wavelengths. For this purpose, four laser diodes (Flexpoint Dot, Laser Components, and Olching, Germany) were arranged annularly around the CCD camera and focused into one single spot, as can be seen in Fig. 2. The laser diodes emit at central wavelengths of 520, 635, 660, and 785 nm at a maximum optical power of 5 mW. The intersection point of all laser beams is located within the object plane of the camera. The measurement procedure was partially automated and implemented in a MATLAB code (MATLAB, The MathWorks Inc., Natick, Massachusetts).

The CCD camera takes an image of the tissue sample surface, while laser light of a single laser diode illuminates a small spot (Ø: ≪0.4 mm) on the sample surface. The procedure is repeated for every laser diode wavelength; hence, one image is generated for every specific wavelength. For evaluation the radial dependence of the light intensity around the laser spot has to be measured; therefore, the light intensity is mapped as a function of the pixel distance from the center of the illuminated light spot.

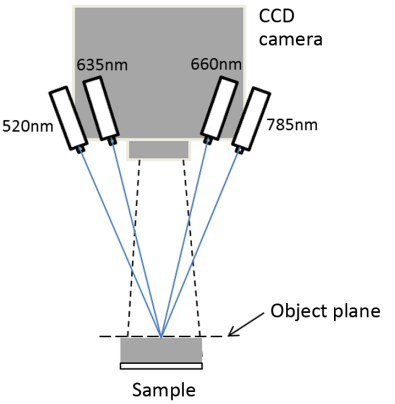

Fig. 2 Spatially resolved reflectance measurement setup comprising a CCD camera and four laser diodes emitting at central wavelengths 520, 635, 660, and 785 nm.

To increase the dynamic range of the remitted light distribution, suitable measures must be taken such that almost every pixel contains a signal clearly distinguishable from the background. To achieve this, images of the light distribution are taken by gradually increasing the integration time of the camera from a minimum value (2 ms), where no pixels are saturated, to a maximum value (5000 ms). Through this step-by-step increase of the integration time, more and more pixels near the spot center become saturated, whereas more and more pixels far from the spot center provide a signal well distinguishable from the background. When considering only unsaturated pixels with signals well above the background and averaging over all respective time-normalized intensities in each of these pixels, a combined gray-scale image with an enhanced dynamic range can be generated. By binning of its pixels into suitably chosen intervals of radial distance from the illumination spot center and averaging over the signal intensities in each bin, a graph of the averaged radial dependence of the diffusely remitted light intensity can be constructed. The sample's effective attenuation coefficient,

$$\mu_{\text{eff}} = \sqrt{3\mu_a(\mu_a + \mu_s')}, \tag{4}$$

can then be determined by fitting a model curve to this graph, based on Monte Carlo simulations with preset values for the scattering anisotropy $g(\lambda_n)$, the refractive index $n_{\text{sample}}(\lambda_n)$ of the sample, and the value $q(\lambda_n)$ determined from the total diffuse reflectance measurements for the respective (laser) wavelength λ_n as described above.[45,46]

2.2.2 *Integrating sphere setup*

The determination of the optical properties using the integrating sphere (IS) was performed, among others, by the indirect spectral measurement of diffuse reflected and transmitted light intensities during illumination of a tissue sample by a white-light source. Subsequently, an IAD procedure[47,48] can be used to evaluate the optical properties μ_a and μ_s', provided that the scattering anisotropy g is predefined. Figure 3 shows exemplarily the setup for the measurement of the diffuse transmitted light.

A xenon arc lamp (D-light, Karl Storz, Tuttlingen, Germany) was coupled into a multimode optical fiber ($Ø_{\text{core}}$: 1.5 mm, NA: 0.37). At the distal end of the fiber the light passes an iris, which was used to adjust the beam diameter and to reduce stray light. A lens (f: 60 mm) focuses the beam onto the sample. Between the distal fiber end and the first iris, a shutter is located and can be used to perform dark measurements for background corrections. The IS (Ø: 101.6 mm, Labsphere North Sutton) is coated with Spectralon®, which has a reflectivity of about 99% in the spectral range from 400 to 1500 nm. The reflected or transmitted diffuse light is detected in the spectral range from 200 to 850 nm via an optical fiber ($Ø_{\text{core}}$: 500 μm, NA: 0.3) attached to a spectrometer (S2000, Ocean Optics, Dunedin) by collecting stray light from the sphere surface within the fiber's numerical aperture.

The spectral determination of the optical properties μ_a and μ_s' of a tissue sample was performed by calculating the diffuse transmission T_d and the diffuse reflectance R_d out of three spectral measurements in counts/ms (Sig_{Td}, Sig_{Rd}, and Sig_{Ref}) in the wavelength range between 400 and 800 nm. The device configurations during the three spectral measurements are shown in Fig. 4.

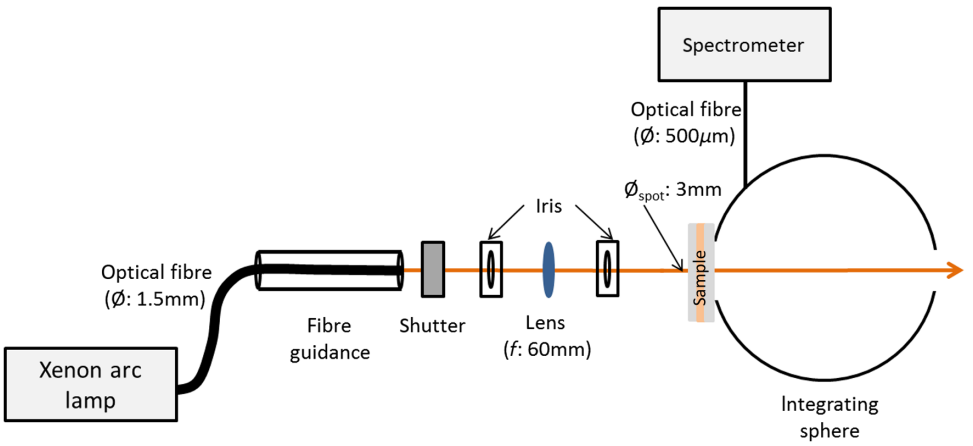

Fig. 3 Schematic setup for the measurement of the diffuse transmitted light passing the sample. Collimated transmitted light leaves the sphere without any interaction.

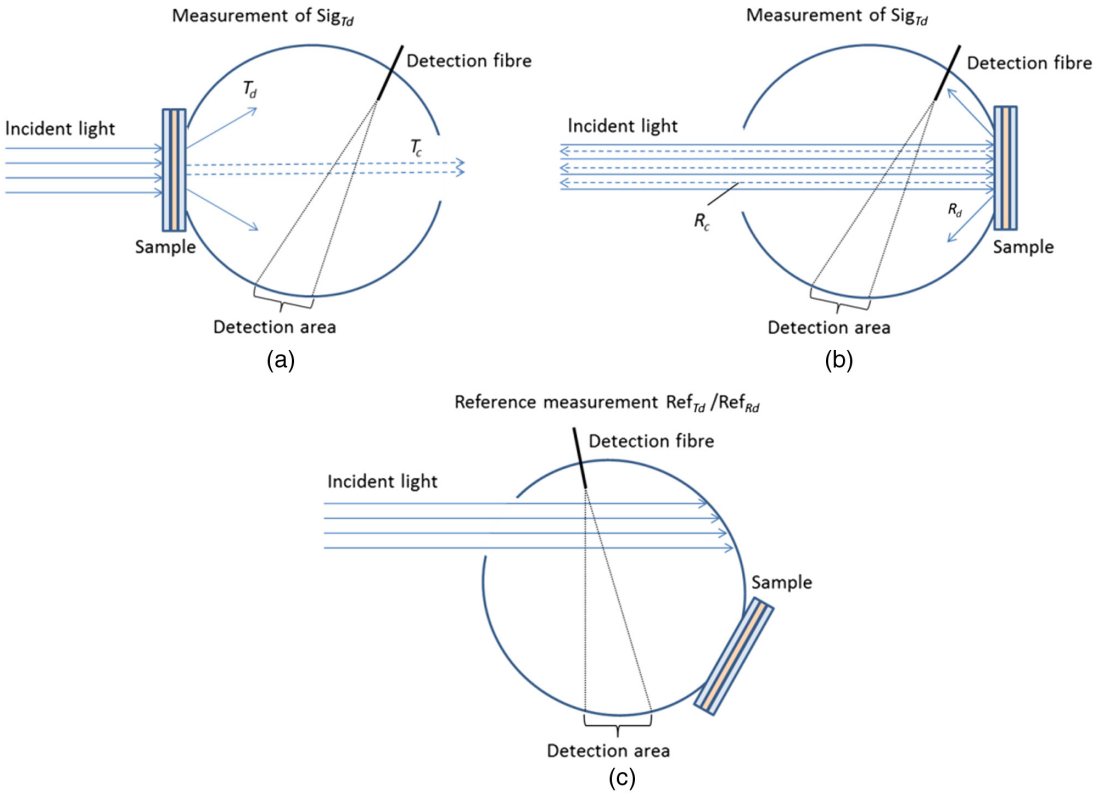

Fig. 4 Top view of the IS for the measurements of (a) Sig_{Td}, (b) Sig_{Rd}, and (c) Sig_{Ref}.

Due to the low collimated transmission signal, it was not possible to determine the anisotropy factor g, which would otherwise be possible with an extended set of measurements (not shown here). As a consequence, μ_s could not be calculated independently; hence, constant literature values were allocated to the scattering anisotropy g and the refractive indices n_{sample} of the sample, namely 0.8[43] and 1.37,[49,50] respectively. Dark spectra (Bg_{Td}, Bg_{Rd}, and Bg_{ref}) were taken and subtracted from the signals as background noise. T_d and R_d can be calculated by the following Eqs. (5) and (6):

$$T_{\mathrm{d}} = \frac{\mathrm{Sig_{Td}} - \mathrm{Bg_{Td}}}{\mathrm{Sig_{Ref}} - \mathrm{Bg_{ref}}} \cdot R_{\mathrm{sphere}}, \tag{5}$$

$$R_{\mathrm{d}} = \frac{\mathrm{Sig_{Rd}} - \mathrm{Bg_{Rd}}}{\mathrm{Sig_{Ref}} - \mathrm{Bg_{ref}}} \cdot R_{\mathrm{sphere}}. \tag{6}$$

The variable R_{sphere} represents the wavelength depending reflectance of the IS's inner coating Spectralon®. Using the inverse adding doubling method established by Prahl et al.,[47,48] the optical properties μ_a and μ_s' can then be computed from T_d and R_d.

2.2.3 *Tissue density measurements*

Mass density measurements were performed on dissected and homogenized tissue samples to identify potential density

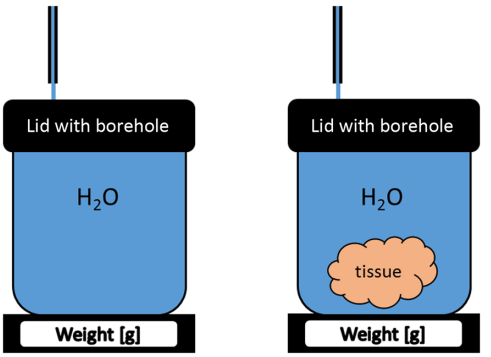

Fig. 5 Experimental setup for density measurement of biological tissue.

changes during the homogenizing process as these may be linked to optical property changes. For every tissue, $n = 5$ density measurements were performed, whereby sample volumes of at least 1 cm^3 were used. For that purpose, a vessel placed on top of a scale (BP 310 S, Sartorius, Göttingen, Germany) (Fig. 5) was filled with water and the corresponding volume (V_w) was determined. Thereupon the vessel was emptied, a volume of tissue had been prepared, its mass m_{sample} had been determined, and then inserted into the vessel, and the scale tared. By filling the vessel with water, the reduced volume V_r can be estimated. The water volume displaced by the sample volume V_{sample} can then be calculated as $\Delta V = V_w - V_r$. The tissue density can then be calculated according to the equation [Eq. (7)] as

$$\rho_{\text{sample}} = \frac{\mathrm{m}_{\text{sample}}}{V}. \tag{7}$$

2.3 *Data Analysis*

The data analysis and representation were performed using Sigma Plot (V.11.0, Systat Software GmbH, Erkrath, Germany). For brevity, abbreviations were used for the four combinations of experimental method and tissue preparation as follows: for the IS setup I and ID in combination with dissected tissue, respectively, IH in combination with homogenized tissue; for the DSR setup R and RD and RH, respectively.

Optical properties were determined for each of the four experiment/preparation combinations, each of the four different laser wavelengths of the DSR setup, and each of the four different tissue types. In each case, the obtained optical properties are graphically represented by mean values (μ_{mean}) out of $n = 5$ measurements, while the error bars represent the corresponding standard errors (μ_{err}). As the IS measurements were performed with a broadband white-light source, the results are shown as full spectra (515 to 800 nm) with error bars at the DSR wavelength positions. The relative standard error, i.e., the ratio of the standard error and the mean value, was evaluated in percent in each case. Afterward, the ratio of the relative standard error for homogenized and dissected tissue was calculated for each case, i.e., for each experimental method, for each wavelength λ, and for each of the four tissue types:

$$(r\lambda;\mathrm{IS}) = \frac{\mu_{\text{err}}(\lambda;\mathrm{IH})/\mu_{\text{mean}}(\lambda;\mathrm{IH})}{\mu_{\text{err}}(\lambda;\mathrm{ID})/\mu_{\text{mean}}(\lambda;\mathrm{ID})}, \tag{8}$$

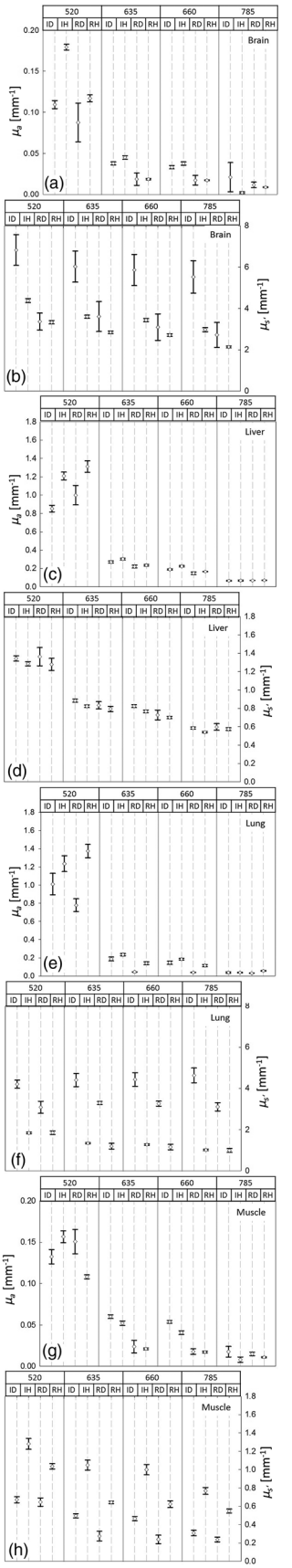

Fig. 6 Optical properties of dissected (ID and RD) and homogenized (IH and RH) brain tissue samples, for the wavelengths 520, 635, 660, and 785 nm. [mean ± stderr ($n = 5$)]. (a) Brain tissue: μ_a, (b) $\mu_{s'}$. (c) Liver: μ_a, (d) $\mu_{s'}$. (e) Lung: μ_a, (f) $\mu_{s'}$. (g) Muscle: μ_a, (h) $\mu_{s'}$.

$$r(\lambda;\mathrm{DSR}) = \frac{\mu_{\mathrm{err}}(\lambda;\mathrm{RH})/\mu_{\mathrm{mean}}(\lambda;\mathrm{RH})}{\mu_{\mathrm{err}}(\lambda;\mathrm{RD})/\mu_{\mathrm{mean}}(\lambda;\mathrm{RD})}. \quad (9)$$

A ratio value $r < 1$ indicates a smaller relative standard error in case of homogenized compared with dissected tissue. Ratio values $r > 1$ indicate that the dissected tissue samples showed smaller relative standard errors. A reference line at $r = 1$ was included in each of these graphs for clarity.

3 Results

3.1 *Optical Property Measurements*

The optical properties obtained for each experiment/preparation combination at the four different wavelengths of the DSR setup are shown in Figs. 6(a)–6(h) for each tissue type (brain, liver, lung, and muscle). The absorption coefficient μ_a is shown in the left column, the reduced scattering coefficient μ_s' in the right column.

In most cases, the absorption coefficient μ_a was found to be higher for homogenized tissues (IH and RH) than for the corresponding dissected tissues (ID and RD). Muscle tissue [Fig. 6(g)] shows the opposite behavior, except at 520 nm, where the IS measurements again yielded a higher μ_a value for homogenized tissue (IH versus ID). Overall, in almost all measurements, the relative standard error decreased using homogenized tissue samples instead of dissected ones.

IS measurements on brain tissue [Fig. 6(b)] (and liver tissue [Fig. 6(d)], with lower significance) yield smaller values for μ_s' in case of homogenized samples. Independent of the experimental method, the same holds for lung tissue [Fig. 6(f)], whereas the opposite behavior is obtained for muscle tissue [Fig. 6(h)]. DSR measurements on brain and liver tissue did not yield significant differences between dissected and homogenized tissue.

For liver tissue, the differences between dissected and homogenized tissue are generally very small, except at a wavelength of 520 nm [Figs. 6(c) and 6(d)].

The comparison of the ratio of relative standard errors of homogenized and the corresponding dissected tissue samples is shown in Fig. 7. The ratio values obtained from IS measurements are shown in the left column, for μ_a in the upper, and μ_s' in the lower graph. The corresponding results obtained from DSR measurements are shown in the right column. As can be seen, the relative standard error for μ_s' was in most cases smaller ($r < 1$) than in the case of homogenized samples, except for lung tissue. For μ_a around one-third of the values were larger

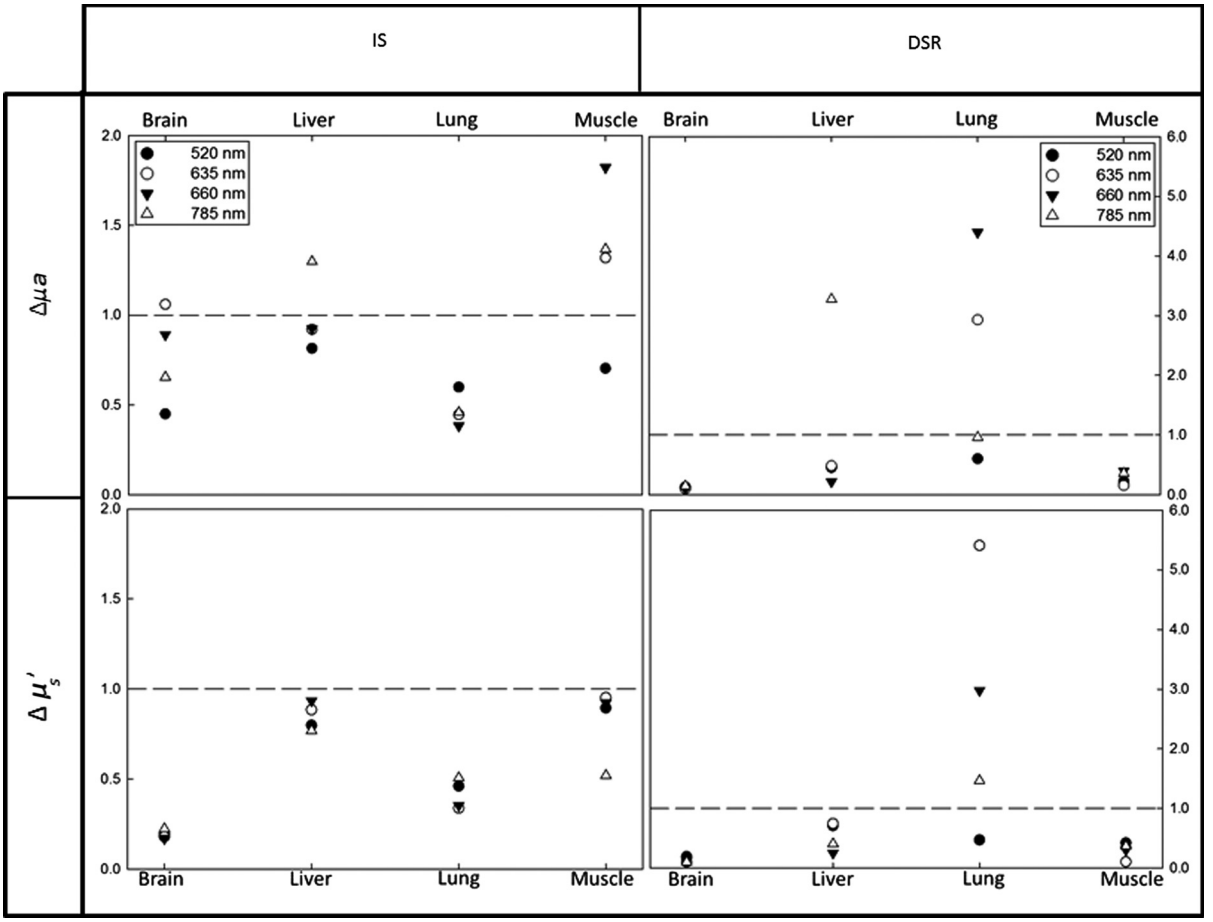

Fig. 7 Ratio of relative standard errors between homogenized and the corresponding dissected tissue samples, plotted for the absorption coefficient and the reduced scattering coefficient in the upper and lower graphs, respectively. Results are shown for the four different source tissues and the four different laser wavelengths of the DSR setup, where results from IS and DSR measurements are collected in the left and right columns, respectively. A ratio value <1 indicates a smaller relative standard error in case of homogenized tissue. Ratio values >1 indicate that the dissected tissue samples showed smaller relative standard errors.

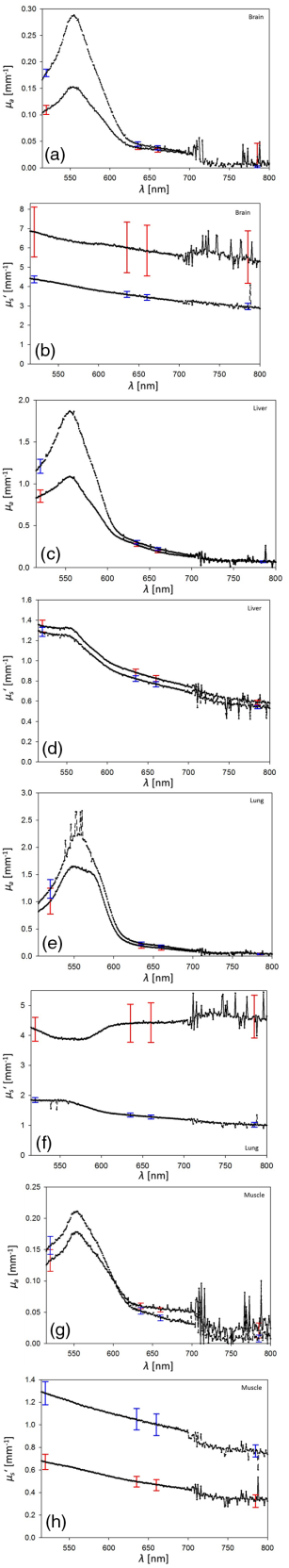

Fig. 8 Mean values ($n = 5$) of the absorption and scattering spectra of the IS measurements (515 to 800 nm). Dissected tissue (solid line) is illustrated with red colored error bars at the DSR wavelength, homogenized samples (interrupted line) with blue error bars at the same wavelength positions, respectively. (a) Brain tissue: μ_a, (b) $\mu_{s'}$. (c) Liver: μ_a, (d) $\mu_{s'}$. (e) Lung: μ_a, (f) $\mu_{s'}$. (g) Muscle: μ_a, (h) $\mu_{s'}$.

Table 1 The results of the tissue density measurements.

	Homogenized ρ (g/cm^3)	Dissected ρ (g/cm^3)	Literature dissected ρ (g/cm^3)
Brain	0.962 to 0.969	1.028 to 1.038	1.030 to 1.041
Liver	1.025 to 1.045	1.068 to 1.082	1.050 to 1.070
Lung	1.012 to 1.018	0.462 to 0.498	0.230 to 1.092
Muscle	1.023 to 1.039	1.069 to 1.093	1.038 to 1.056

($r > 1$) than one and hence had smaller relative standard errors for dissected tissue.

The IS mean values ($n = 5$) for the absorption and scattering coefficient for both preparation methods derived from IS investigations (mean of $n = 5$) in the spectral range from 515 to 800 nm are shown in Figs. 8(a)–8(h). Measurements performed with dissected tissue are displayed as solid lines with red colored error bars at the DSR wavelength positions, for homogenized samples interrupted lines and blue error bars were used. Absorption coefficients [Figs. 8(a), 8(c), 8(e), and 8(g)] are increased for homogenized tissue samples in comparison with dissected in the spectral range of 515 to 580 nm, and become aligned from 580 to 800 nm. The scattering coefficient values for homogenized samples mostly lay below the ones for dissected [Figs. 8(b), 8(d), and 8(f)], except for muscle [Fig. 8(h)]. The smallest deviation depending on preparation method could be observed for liver [Fig. 8(d)]; additionally, the revealed results for absorption and reduced scattering are in good relation to Roggan et al.[43] In the most graphs, except for μ_s' [Fig. 8(h)] and μ_a [Fig. 8(g)] of muscle tissue, the standard deviations were smaller or at least very similar in comparison with the error bars of dissected tissue. This agrees very well with the results of the relative errors of the IS measurements shown in Fig. 7.

3.2 *Tissue Density Measurements*

The results of the tissue density measurements are listed in Table 1 and compared with literature values.[51] In the case of lung tissue, the obtained results were compared with both deflated and inflated lung tissue; in the case of muscle tissue, to skeletal muscle tissue. For all types of tissue, except lung, a decrease in the mass density was observed upon homogenization. The values for dissected tissue correspond well with the literature data.

4 Discussion

The optical properties of different types of homogenized and dissected porcine tissue samples (brain, liver, lung, and muscle) were determined using IS and DSR measurements. In the case of homogenized tissue, a reduction in the relative standard error of the obtained optical coefficients was observed, which can be attributed to an improved reproducibility of the experiments. Furthermore, the improved reproducibility can be attributed to the destruction of internal tissue structures, so that extreme local changes[33] in the optical properties of the specific tissue sample can be overcome. This seems to be a fact for all tissues investigated except for lung samples (Fig. 7), which might be traced back to incomplete homogenizing within the 2 min shredding. Overall, using homogenized tissue samples, the

preparation of the samples was much easier, and the performance of the experiments was less time consuming. All in all, homogenization of tissues for *ex vivo* experiments using standard setups like IS or diffuse reflectance analysis seems to be a promising way to create stable and reproducible datasets of the optical properties of different tissues. However, one has to consider whether the gained results of such a methodology are suitable for the particular clinical application.

It can be derived that the absorption coefficient is increased for homogenized tissue samples in comparison with the corresponding sliced tissue, which can be explained by a more even distribution of blood cells within the tissue sample. Red blood cells are one of the main absorbers in tissues,[7] whereby the increased μ_a values in the spectral range of 500 to 580 nm can be explained.[43,52] In contrast to the dissected samples, where blood is concentrated in certain areas and vessels, the blood will be spread fairly evenly over the whole sample volume upon homogenization. This may lead to a higher μ_a from 400 to 600 nm as seen in the IS spectral data [Figs. 8(a), 8(c), 8(e), and 8(g)] and can be related to an effect known as pigment packaging.[53] Equally, the destruction of internal structures changes the scattering coefficient in comparison with the sliced sample due to altering of local nonuniformities in the microstructure, e.g., the size, shape, and orientation as well as the refractive index mismatch of the scattering particles.[54]

The homogenization process also raises issues like how the changes in tissue morphology, namely the introduction or extraction of air, in addition to the redistribution of tissue fluids or other tissue constituents, may influence the absorption and scattering coefficients measurable on the sample.[54] Therefore, mass density measurements were performed additionally to assess the extent of such morphological changes induced by the used tissue homogenization procedure.

Within the experimental errors, the measured mass densities of the dissected tissue samples were quite consistent with the corresponding literature values. The wide range of literature values in the case of lung tissue can be explained by the potentially high air content in the tissue. For full inflation, densities around 0.23 g/cm^3 are found in the literature, whereas for deflation the density is reported to increase to around 1.09 g/cm^3. The performed density measurements on dissected lung tissue yielded values of around 0.480 g/cm^3, which is intermediate between the two extreme values reported in the literature.[51]

In all cases, despite lung tissue, homogenizing of the tissue samples lead to a decrease in density. This might be explained by destroying denser structures and simultaneously inserting air into the sample due to the mixing procedure. Such an effect could potentially be avoided by performing the homogenization in vacuum. Lung tissue, on the other hand, becomes a lot denser (from 0.480 to 1.015 g/cm^3) upon homogenization, which might be due to a removal or destruction of the air inclusions in the lung tissue. In the case of muscle tissue, the opposite effect is observed, whereby rather well-aligned supporting structures within muscle tissue are destroyed; upon homogenization, these "boundaries" are strongly disturbed so that they strongly scatter the impinging light.[18,33,52] The performed tissue preparation may affect the determined optical properties. Although the destruction of the structure may influence the absorption and reduced scattering coefficient, packaging effects and blood distribution may alter mainly the absorption coefficient, and the preparation related density changes may have influences on both parameters.

The advantages tissue homogenization compared to tissue slices is that even small samples become usable for the determination of its optical properties. This applies especially to the IS measurement technique, where the sample size and thickness do not need to be particularly large.[55] Hence, after homogenizing the tissue, a thin layer of the disintegrated tissue can be spread between two glass slides whose distance can be quite small. One only has to ensure that the sample port is fully covered and that the sample is not squeezed. Regarding experimental aspects, homogenization allows for a much faster and easier sample preparation, due to the fact that no preparation time is required for a suitable tissue dissection aiming for an increase in reproducibility of the optical property data.

5 Conclusion

The optical properties of tissue samples were investigated and compared for homogenized versus dissected tissues. The comparison of the data showed good agreement for μ_s', while the μ_a differences were probably influenced by blood. Experiments using homogenized tissue samples show high reproducibility and are less time consuming. Further investigations should be performed to statistically proof the statement.

Disclosures

The authors have no financial interests in this article and no potential conflicts of interest to disclose. All tissues were received from local abattoir. Thus, no animal experiments were performed and no animal was sacrificed especially for the experiments. In principle, the tissues examined are generally sold for public consume.

Acknowledgments

This manuscript was part of the inaugural thesis of Maximilian Eisel to be submitted at the Medical Faculty of the Ludwig-Maximilians-Universität, Munich.

References

1. D. E. Dolmans, D. Fukumura, and R. K. Jain, "Photodynamic therapy for cancer," *Nat. Rev. Cancer* **3**(5), 380–387 (2003).
2. T. J. Dougherty et al., "Photodynamic therapy," *J. Natl. Cancer Inst.* **90**(12), 889–905 (1998).
3. H. I. Pass, "Photodynamic therapy in oncology: mechanisms and clinical use," *J. Natl. Cancer Inst.* **85**(6), 443–456 (1993).
4. M. Burger et al., "Photodynamic diagnostics and noninvasive bladder cancer: is it cost-effective in long-term application? A Germany-based cost analysis," *Eur. Urol.* **52**(1), 142–147 (2007).
5. S. Denzinger and M. Burger, "Photodynamic diagnostics of bladder tumors," *Curr. Urol. Rep.* **9**(2), 101–105 (2008).
6. E. K. Chan et al., "Effects of compression on soft tissue optical properties," *IEEE J. Sel. Top. Quantum Electron.* **2**(4), 943–950 (1996).
7. S. L. Jacques, "Optical properties of biological tissues: a review," *Phys. Med. Biol.* **58**(11), R37–R61 (2013).
8. S. Andersson-Engels et al., "In vivo fluorescence imaging for tissue diagnostics," *Phys. Med. Biol.* **42**(5), 815–824 (1997).
9. J. Hegyi et al., "New developments in fluorescence diagnostics," *J. Dtsch Dermatol. Ges.* **9**(5), 368–372 (2011).
10. D. W. Burden, "Guide to the disruption of biological samples-2012," *Random Primers* **12**(12), 1–25 (2012).
11. E. Salomatina and A. N. Yaroslavsky, "Evaluation of the in vivo and ex vivo optical properties in a mouse ear model," *Phys. Med. Biol.* **53**(11), 2797–2807 (2008).
12. Y. Peng and S. Dhakal, "Optical methods and techniques for meat quality inspection," *Trans. Am. Soc. Agric. Biol. Eng.* **58**, 1371 (2015).

13. A. Kim and B. C. Wilson, "Measurement of ex vivo and in vivo tissue optical properties: methods and theories," in *Optical-Thermal Response of Laser-Irradiated Tissue*, A. J. Welch and M. J. C. Van Gemert, Eds., pp. 267–319, Springer, Dordrecht, Netherlands (2010).
14. J. F. Beek et al., "In vitro double-integrating-sphere optical properties of tissues between 630 and 1064 nm," *Phys. Med. Biol.* **42**(11), 2255–2261 (1997).
15. J. W. Pickering et al., "Double-integrating-sphere system for measuring the optical properties of tissue," *Appl. Opt.* **32**(4), 399–410 (1993).
16. T. L. Troy and S. N. Thennadil, "Optical properties of human skin in the near infrared wavelength range of 1000 to 2200 nm," *J. Biomed. Opt.* **6**(2), 167–176 (2001).
17. A. N. Yaroslavsky et al., "Optical properties of selected native and coagulated human brain tissues in vitro in the visible and near infrared spectral range," *Phys. Med. Biol.* **47**(12), 2059–2073 (2002).
18. B. Aernouts et al., "Effect of ultrasonic homogenization on the Vis/NIR bulk optical properties of milk," *Colloids Surf., B* **126**, 510–519 (2015).
19. A. López-Maestresalas et al., "Bulk optical properties of potato flesh in the 500–1900 nm range," *Food Bioprocess Technol.* **9**(3), 463–470 (2016).
20. Y. Villanueva, C. Veenstra, and W. Steenbergen, "Measuring absorption coefficient of scattering liquids using a tube inside an integrating sphere," *Appl. Opt.* **55**(11), 3030–3038 (2016).
21. F. Foschum, M. Jager, and A. Kienle, "Fully automated spatially resolved reflectance spectrometer for the determination of the absorption and scattering in turbid media," *Rev. Sci. Instrum.* **82**(10), 103104 (2011).
22. F. Foschum and A. Kienle, "Broadband absorption spectroscopy of turbid media using a dual step steady-state method," *J. Biomed. Opt.* **17**(3), 037009 (2012).
23. S. Jacques, "Video reflectometry to specify optical properties of tissue in vivo," *Proc. SPIE* **10311**, 103110D (1993).
24. A. Kienle et al., "Spatially resolved absolute diffuse reflectance measurements for noninvasive determination of the optical scattering and absorption coefficients of biological tissue," *Appl. Opt.* **35**(13), 2304–2314 (1996).
25. A. Wang, R. Lu, and L. Xie, "Improved algorithm for estimating the optical properties of food products using spatially-resolved diffuse reflectance," *J. Food Eng.* **212**, 1–11 (2017).
26. J. J. Xia et al., "Characterizing beef muscles with optical scattering and absorption coefficients in VIS-NIR region," *Meat Sci.* **75**(1), 78–83 (2007).
27. R. L. P. van Veen et al., "Determination of VIS-NIR absorption coefficients of mammalian fat, with time- and spatially resolved diffuse reflectance and transmission spectroscopy," in *Biomedical Topical Meeting*, Miami Beach, Florida, Optical Society of America (2004).
28. M. S. Patterson, B. Chance, and B. C. Wilson, "Time resolved reflectance and transmittance for the noninvasive measurement of tissue optical properties," *Appl. Opt.* **28**(12), 2331–2336 (1989).
29. M. S. Patterson et al., "Frequency-domain reflectance for the determination of the scattering and absorption properties of tissue," *Appl. Opt.* **30**(31), 4474–4476 (1991).
30. E. R. Anderson, D. J. Cuccia, and A. J. Durkin, "Detection of bruises on golden delicious apples using spatial-frequency-domain imaging," *Proc. SPIE* **6430**, 64301O (2007).
31. A. I. Kholodnykh et al., "Precision of measurement of tissue optical properties with optical coherence tomography," *Appl. Opt.* **42**(16), 3027–3037 (2003).
32. V. V. Tuchin, *Optical Clearing of Tissues and Blood*, SPIE Press, Bellingham, Washington (2006).
33. E. A. Genina et al., "Effect of storage conditions of skin samples on their optical characteristics," *Opt. Spectrosc.* **107**(6), 934–938 (2009).
34. D. B. MacDougall, "Changes in the colour and opacity of meat," *Food Chem.* **9**(1), 75–88 (1982).
35. B. M. Nicolaï et al., "Nondestructive measurement of fruit and vegetable quality by means of NIR spectroscopy: a review," *Postharvest Biol. Technol.* **46**(2), 99–118 (2007).
36. A. Pitzschke et al., "Optical properties of rabbit brain in the red and near-infrared: changes observed under in vivo, postmortem, frozen, and formalin-fixated conditions," *J. Biomed. Opt.* **20**(2), 025006 (2015).
37. K.-B. Sung et al., "Accurate extraction of optical properties and top layer thickness of two-layered mucosal tissue phantoms from spatially resolved reflectance spectra," *J. Biomed. Opt.* **19**(7), 077002 (2014).
38. N. Honda et al., "Optical properties of tumor tissues grown on the chorioallantoic membrane of chicken eggs: tumor model to assay of tumor response to photodynamic therapy," *J. Biomed. Opt.* **20**(12), 125001 (2015).
39. M. S. Wróbel et al., "Nanoparticle-free tissue-mimicking phantoms with intrinsic scattering," *Biomed. Opt. Express* **7**(6), 2088–2094 (2016).
40. M. S. Wróbel et al., "Measurements of fundamental properties of homogeneous tissue phantoms," *J. Biomed. Opt.* **20**(4), 045004 (2015).
41. H. Sajjadi, "Endoscopic middle ear and mastoid surgery for cholesteatoma," *Iranian J. Otorhinolaryngol.* **25**(71), 63–70 (2013).
42. D. W. Roberts and J. Olson, "Fluorescein guidance in glioblastoma resection," *New Engl. J. Med.* **376**(18), e36 (2017).
43. A. Roggan et al., "The effect of preparation technique on the optical parameters of biological tissue," *Appl. Phys. B* **69**(5), 445–453 (1999).
44. S. Doizi and O. Traxer, "Re: evaluation of a novel single-use flexible ureteroscope," *Eur. Urol.* **72**(1), 152–153 (2017).
45. M. Pilz, S. Honold, and A. Kienle, "Determination of the optical properties of turbid media by measurements of the spatially resolved reflectance considering the point-spread function of the camera system," *J. Biomed. Opt.* **13**(5), 054047 (2008).
46. T. J. Beck et al., "Clinical determination of tissue optical properties in vivo by spatially resolved reflectance measurements," in *Photon Migration and Diffuse-Light Imaging*, Munich, Optical Society of America (2003).
47. S. Prahl, "Optical property measurements using the inverse adding doubling program," (2011).
48. S. A. Prahl, M. J. C. van Gemert, and A. J. Welch, "Determining the optical properties of turbid media by using the adding-doubling method," *Appl. Opt.* **32**(4), 559–568 (1993).
49. F. P. Bolin et al., "Refractive index of some mammalian tissues using a fiber optic cladding method," *Appl. Opt.* **28**(12), 2297–2303 (1989).
50. J. J. Dirckx, L. C. Kuypers, and W. F. Decraemer, "Refractive index of tissue measured with confocal microscopy," *J. Biomed. Opt.* **10**(4), 44014 (2005).
51. F. A. Duck, *Physical Properties of Tissues: A Comprehensive Reference Book*, Academic Press Inc., San Diego, California (1990).
52. D. Cozzolino, D. De Mattos, and D. V. Martins, "Visible/near infrared reflectance spectroscopy for predicting composition and tracing system of production of beef muscle," *Anim. Sci.* **74**(3), 477–484 (2002).
53. J. C. Finlay and T. H. Foster, "Effect of pigment packaging on diffuse reflectance spectroscopy of samples containing red blood cells," *Opt. Lett.* **29**(9), 965–967 (2004).
54. R. Van Beers et al., "Evolution of the bulk optical properties of bovine muscles during wet aging," *Meat Sci.* **136**, 50–58 (2018).
55. E. Chan, T. Menovsky, and A. J. Welch, "Effects of cryogenic grinding on soft-tissue optical properties," *Appl. Opt.* **35**(22), 4526–4532 (1996).

Maximilian Eisel began his studies in applied physics at the University of Applied Sciences Munich after finishing school in 2009, and finished his bachelor degree after completing his thesis at Truma GmbH in 2014. Afterwards he received his master's degree in photonics at the University of Applied Sciences in 2016, by finishing his master's thesis at the Laser-Forschungslabor (LFL) in the LIFE-Center of the University Hospital of Munich. Since, that time he is a PhD student at the LFL working on investigations to improve clinical laser induced lithotripsy.

Ronald Sroka is the head of the LFL at the LIFE-Center of the University Hospital of Munich. He is mostly engaged in the research and development of fluorescence diagnosis, photodynamic therapy and laser surgery in nearly all medical disciplines focusing on the translational technical implementation of several laser applications into the clinics. He is the general secretary of the German Society of Lasermedicine (DGLM e.V.) and executive member of the ELA. Since 2015, he is adjunct professor and advisory board member of the Institute of Photomedicine Tongji-University Shanghai.

Biographies for the other authors are not available.